Enhanced in vitro cytotoxicity and cellular uptake of DNA bases functionalized gold nanoparticles in HeLa cell lines

ARTICLE *in* RSC ADVANCES · JANUARY 2015

Impact Factor: 3.84 · DOI: 10.1039/C4RA15356A

3 AUTHORS:

Shubhangi Borse
Savirtibai Phule Pune University
3 PUBLICATIONS **4** CITATIONS
SEE PROFILE

Satyawati Sudhir Joshi
Savirtibai Phule Pune University
40 PUBLICATIONS **622** CITATIONS
SEE PROFILE

Ayesha Khan
Savirtibai Phule Pune University
23 PUBLICATIONS **162** CITATIONS
SEE PROFILE

RSC Advances

PAPER

View Article Online
View Journal | View Issue

Cite this: *RSC Adv.*, 2015, **5**, 13402

Enhanced *in vitro* cytotoxicity and cellular uptake of DNA bases functionalized gold nanoparticles in HeLa cell lines†

Shubhangi Borse, Satyawati Joshi* and Ayesha Khan

The aggregation of nanoparticles (NPs) in the tumour environment has been hypothesized to enhance retention and cellular uptake, crucial for NP-assisted cancer treatment. Gold nanoparticles (AuNPs) are synthesized by reducing gold chloride with sodium borohydride and are appended with mono and paired DNA bases (adenine, cytosine, and thymine). The AuNPs–DNA base nanoconjugates show aggregation which was characterized by UV-Vis spectroscopy and TEM. An intense surface plasmon resonance (SPR) band in the visible region at 520 nm was observed for the synthesized AuNPs, while addition of mono and pair of DNA bases exhibited colour change and generation of a new band at higher wavelengths. FTIR studies evidenced the mode of interaction of the DNA bases with the AuNPs. A zeta-potential study indicates that functionalized AuNPs were negatively charged and showed zeta-potential values in the range of −53 to −24.5 mV. These functionalized AuNPs were internalized to a greater extent with high cellular uptake than AuNPs into HeLa cells, quantitatively examined using MP-AES and visualized by optical microscopy. MP-AES results estimated the highest (51.43%) cellular uptake for AuNPs–CT among other NPs. A cytotoxicity study demonstrates that functionalized AuNPs possess a higher toxicity than AuNPs against HeLa cells.

Received 27th November 2014
Accepted 20th January 2015

DOI: 10.1039/c4ra15356a

www.rsc.org/advances

Introduction

Recently nanoparticles (NPs) have gained impetus in biomedical applications for the diagnosis and treatment of various diseases. A specific targeting strategy has been achieved *via* ligands targeting receptors that are over-expressed on the diseased cells.[1] Enhanced tumour targeting, improved cancer bearing survival time, and reduced side-effects *in vivo* and tumour cell uptake *in vitro* have been some of the major outcomes. Doxorubicin-loaded targeted polymeric NPs (BIND-014), are one of the successful examples and are currently under clinical evaluation.[2]

Among the targeted strategies in the utilization of nanoparticles one class of inorganic particles that has shown promise in targeted cancer therapy is gold nanoconstructs.[3] Gold nanoparticles (AuNPs) can be synthesized with very precise sizes, shapes and surface chemistry at the nanoscale level.[4] Besides the physical and chemical properties of AuNPs, they are easily characterized by UV-Vis spectrometry and microscopy, while their unique optical properties make them particularly attractive tools for cancer detection and therapy.[5] The ability to collectively oscillate their conduction-band electrons during light exposure, AuNPs can scatter light resulting in an array of colours characteristic of colloidal gold.[6] These properties have recently been exploited for early detection of cancer biomarkers.[7,8] If gold nanoparticles, particularly rods, are exposed to wavelengths dictated by the particles aspect ratio, then surface plasmon resonance may occur and the light energy is transformed into heat.[5,6] This phenomenon has led to the idea of using gold nanorods to target tumors and thermally ablate them using near-infrared (NIR) light irradiation.[9–11]

AuNPs have the advantage of small size, which is highly tunable (1–100 nm), enabling them to evade the immune system. The optical properties of AuNPs, such as surface plasmon resonance, provide excellent fluorescence and photostability necessary for imaging applications.[12,13] The chemical properties of AuNPs, such as chemical inertness, low toxicity to human cells,[14] and high selectivity,[15] allow them to interact easily with the biological systems. AuNPs have been used to deliver antitumor agents such as tumour necrosis factor (TNF) or paclitaxel at the site of the tumour by the enhanced permeability and retention (EPR) effect.[16]

Surface modification of metal particles using functionalized capping molecules has led to exciting possibilities for anchoring colloidal particles to metal surfaces. Recently, this has also been exploited in the development of diagnostic tools for biological compounds. AuNPs when functionalized with the

Department of Chemistry, Savitribai Phule Pune University, Pune-411007, India. E-mail: ssjoshi@chem.unipune.ac.in; Fax: +91-020-25691728; Tel: +91-020-25601394 ext. 573/569/532

† Electronic supplementary information (ESI) available: Zeta potential data, FTIR data, structure of adenine, thymine and cytosine and their pairs and cytotoxicity study of healthy cells line. See DOI: 10.1039/c4ra15356a

suitable surface moieties, can readily penetrate living cells.[17] Therefore, attempts have been made to stabilize metal nanoparticles in the presence of biologically important compounds such as DNA, DNA bases and proteins.[18–21] DNA bases are the fundamental constituent of nucleic acids containing nitrogen found within nucleotides. Thus interaction of metal nanoparticles with nucleic acids is important in the bioinorganic field because of its imminent effects on the synthesis, replication, and structural integrity of DNA and RNA.[22] After proteins, the nucleic acids are the most studied biomolecules for capping noble metal nanoparticles. Cytosine modified Gd_2S_3:Eu^{3+} nanoparticles show better accumulation of blood platelets with cytosine modified nanoparticles as compared to unmodified NPs.[23] Rotello and co-workers have synthesized functionalized AuNPs which carry oligonucleotides inside the cell.[24] Several researchers have been able to modify the AuNPs surface for enhanced applicability. Amongst this thiol modification and DNA bases have been able to modulate the chemical and physical characteristics. The formation of a polymeric network of DNA–AuNPs by mixing two oligonucleotide-functionalized AuNPs probes with a solution of DNA target results in a concomitant red-to-purple colour change. Furthermore, DNA-modified AuNPs have been used for the colorimetric detection of duplex and triplex DNA binding molecules.[25–27] Some purine derivatives (Pds) such as xanthine and uric acid were reported to block the growth of AuNPs, which may attribute to the formation of Pds–Au(III) complexes.[28] Different Pds have different affinities to the Au(III) ion. However, it is still unclear how ligand–Au(III) affinities affect the growth of AuNPs. A better understanding of the AuNPs–biomolecule interactions would inspire new ideas for the development of AuNPs-based bioassays.

The present study investigates the cellular uptake of AuNPs appended with DNA bases such as adenine, thymine and cytosine. Similarly, a pair of DNA bases such as AuNPs with adenine–thymine and a mismatch pair cytosine–thymine and adenine–cytosine were synthesized and characterized by their physico-chemical studies. In the present study HeLa cell lines were selected to study the cytotoxicity of the AuNPs and other DNA base conjugates. Although other immortalized lines are vastly available, HeLa remains the most widely used cell line in biomedical research. HeLa cells can be used to explore the complex processes involved in the growth, differentiation, and cell death processes. Pair of bases appended AuNPs show excellent cytotoxicity as well as high cellular uptake for human cervical cancer cell line.

Experimental

Materials

All the chemicals used were of analytical grade. Chloroauric acid ($HAuCl_4 \cdot 3H_2O$) (Thomas Baker, India), sodium borohydride (Merck, India), cytosine, adenine, thymine, agarose (Sigma-Aldrich, India), tris base (Merck, India), boric acid (Merck, India), and EDTA (Merck, India), were used without further purification. Milli-Q water was used throughout the course of the investigation.

Synthesis of gold nanoparticles

Gold nanoparticles were prepared by reduction of 1 mM chloroauric acid [$HAuCl_4$] with 2 mM ice-cold sodium borohydride [$NaBH_4$] solution.[29,30] A 1 : 1 ratio of [$NaBH_4$] and [$HAuCl_4$] resulted in the breakdown of the product within an hour. Thus a reaction optima was obtained with the initial ratio of [$NaBH_4$]/[$HAuCl_4$] = 2.0. Briefly the solution of chloroauric acid was vigorously stirred with the sodium borohydride solution for an hour at room temperature. Initially the mixture formed an orange colour which subsequently, turned black in few minutes and this was, persistent up to 15 to 20 min. Finally, the product obtained was ruby red colour. The pH of the colloidal solution was also checked.

Synthesis of DNA bases functionalized AuNPs

Stock solutions of DNA bases (20 mM) and pair of DNA bases (20 mM) were prepared in Milli-Q water. An aliquot of each of the DNA base and pair of DNA bases solution (30 μL) was added to the gold colloidal solution (3 mL). The colour changed from red to blue/violet/purple depending on the DNA bases/pair of DNA bases, indicating the formation of DNA bases functionalized AuNPs. Interaction with guanine could not be studied due to its low solubility in water. The pH of the solution was checked after the addition of DNA bases.

Gel electrophoresis

A 0.2% agarose gel was prepared by heating 300 mg of agarose in 150 mL of 0.5× TBE buffer and allowed to cool at 60 °C prior to pouring the gel. The 0.5× TBE buffer was prepared by diluting a 5× TBE buffer stock solution (54 g tris base, 27.5 g boric acid, and 20 mL 0.5 M EDTA, pH 8.0, per L). Samples consisting of 40 μL DNA bases functionalized AuNPs and 5 μL glycerol/deionized water (1 : 1, v/v) were loaded into the wells. The gels were run in a horizontal electrophoresis system (Midi-Horizontal System Bio Era) at 50 V for 1 h.

Isolation of healthy cells from mouse spleen

Specific pathogen free BALB/c mice was selected. The mouse was killed by cervical dislocation.[31] Complete medium was placed in a Petri dish while the dish was placed at an angle by resting it partially on its lid. A hole in the capsule was made using forceps, at one end of the spleen. The spleen was placed on the sloping Petri dish, punctured end facing down. Using a cell scraper gently press cells out of the spleen by working the scraper from the middle to the lower end of the spleen. Another hole at the other end of it was made and the rest of the cells were removed out. When all cells were removed, the empty capsule was discarded and the cells were transferred to a conical tube. The volume was adjusted appropriately. The cells were cultured in a T-25 flasks with RPMI-1640 (Sigma; cat. no. R-7638) supplemented with 10% heat-inactivated fetal calf serum (FCS), 2 mM L-glutamine, 100 U mL^{-1} penicillin/streptomycin, and 5 × 10^{-5} M 2-mercaptoethanol (2 ME).

Testing of functionalized AuNPs against HeLa and healthy cells

The cells were seeded from the T-flask and added to a 96-well plate. 1 mL of 1×10^5 cells per mL medium and with varying concentration of the compounds were added and kept in the CO_2 incubator. After 24, 48, 72, and 96 h MTT assays were done to check the cell viability. All experiments were carried out in Laminar flow hoods, Laminar Flow Ultraclean Air Unit, Micro filter, India. The cells were visualized using an Inverted Microscope, Olympus.

Cytotoxicity studies

Cytotoxicity studies were evaluated in the HeLa cell line obtained from National Centre for Cell Science (NCCS), Pune University, Pune, India. Cell viability was tested using the 3-(4,5-dimethylthiazol-2-yl)-2,5-diphenyltetrazolium bromide (MTT) assay. The cells were seeded in a 24–well plate at a density of 10^4 cells per well in Dulbecco's Modified Eagle's Medium (DMEM) containing 10% fetal calf serum and a 0.1% antibiotic solution for 24 h at 37 °C and 5% CO_2 for adherence. Functionalized AuNPs (5–100 μg mL^{-1}) were dispersed in 1% DMSO and added to the wells with fresh medium. 1% DMSO was used as a vehicle control. After every 24, 48, 72 and 96 h of incubation, MTT assay was carried out. The MTT solution (20 μL, 5 mg mL^{-1}) prepared in a 10 mM phosphate buffer was added to each well and incubated for 4 h. The purple formazan product was dissolved by addition of 100 μL of 100% DMSO for 5 min. The absorbance was measured at 570 and 630 nm using an ELISA plate reader, and the viability was calculated. Data were collected for three replicates each and were used to calculate the mean. The percentage inhibition was calculated from this data:

$$\%\ \text{Inhibition} = \frac{\text{Mean OD of untreated cells (control)}}{\text{Mean OD of treated cells (control)}} \times 100$$

Quantification of internalized functionalized AuNPs by MP-AES

The cell suspension was stored at −20 °C until analysis. For the uptake studies by microwave plasma atomic emission spectroscopy (MP-AES) HeLa cells were grown in a 6 well plate and incubated for 24 h with 100 μL functionalized AuNPs. Cells were washed three times with PBS to remove NPs not associated with the cells before sample collection. 0.15 mL of aqua regia (3 : 1 hydrochloric acid : nitric acid [caution must be taken when handling, as reactions are exothermic]) was added to 10 μL of cell of solution. This solution was incubated for overnight, then further diluted to 5 mL using Milli Q water to give a total sample volume of 5 mL. These samples were then analyzed for total gold content by MP-AES, and the measurement was repeated 3 times for each sample. An Agilent 4100 MP-AES was used, and values reported were based on a calibration curve using an Au MP-AES standard. The emission Au line used was at 267.59 nm. The gold concentration, the calculated number of accumulated AuNPs, the normalized number of AuNPs per cell and the accumulation percentage is reported in the main text.

Staining of cells for detection of changes in morphology

HeLa cells (10^4) were cultured on cover slips for 24 h and incubated after treating with nanoparticles conjugated with FITC for another 4 h. The treated cover slips were transferred into another 6-well plate where the cells were fixed with 1% paraformaldehyde. Next, DAPI stain was added for 3–5 min. Cover slips were washed with PBS to remove excess stain. The cover slip was dipped in alcohol and was allowed to dry. The cover slip was dipped in xylene and mounted using DPX. The images were captured using Carl Zeiss Axio Scope A1 fluorescent microscope with filter set number FS3 excitation at 340 nm.

The optical absorption spectra of colloidal solutions were recorded on UV-1800 (Shimadzu) UV-visible spectrophotometer. Infrared spectra were recorded on FTIR 8400 (Jasco) spectrophotometer. Sampling was done using a KBr pellet. An Agilent 4100 MP-AES was used for the quantification of gold nanoparticles. TEM analysis was carried out on PHILIPS CM 200 operated at 80 kV. The samples were prepared by dropping 2 μL gold colloid particle solutions onto a 400-mesh icon carbon-coated copper grid and wicking off the excess sample with filter paper after 30 seconds and drying at room temperature. Statistics describing the size distribution of the observed colloids was analyzed by counting 100 particles. The zeta potential was measured at 25 °C using Malvern Zetasizer Nano ZS instrument. Briefly, the samples were loaded into a pre-rinsed folded capillary cell and a voltage of 150 and 100 V was applied. The zeta potential measurements were made in triplicates.

Results and discussion

Results

UV-visible absorption spectroscopy is the most widely used method for characterizing the optical properties and electronic structure of nanoparticles, as the absorption bands are related to the diameter and aspect ratio of metal nanoparticles. The time-dependent aggregation data were taken to understand the kinetics of gold assembly formation *via* recording the time-dependent UV-visible spectra of the colloidal gold after addition of 30 μL cytosine (20 mM) at room temperature (Fig. 1A). The intensity of 520 nm decreased with slight bathochromic shift (527 nm), and a new plasmon band at 658 nm appeared, while the colour changed from red to deep blue (inset Fig. 1A). However, precipitation accrued within 1 h after the addition of cytosine in AuNPs, with a zeta potential value of −31.8 mV. This indicated moderate stability of the solution (Fig. S1, ESI†). While upon addition of 30 μL thymine (20 mM), the intensity of the band at 520 nm gradually decreased, and a new plasmon band at 636 nm increased exponentially, indicating the formation of thymine–gold assembly (Fig. 1B), with the colour change from red to violet (inset Fig. 1B). In the AuNPs–T assembly precipitation accrued after 10 days. Moreover AuNPs–T has a zeta potential of −41.8 mV, which indicates good stability of the solution (Fig. S1, ESI†). The addition of 30 μL adenine (20 mM) in colloidal gold solution shows broad band at 580 nm (Fig. 1C), with the colour change from red to violet (inset Fig. 1C). The

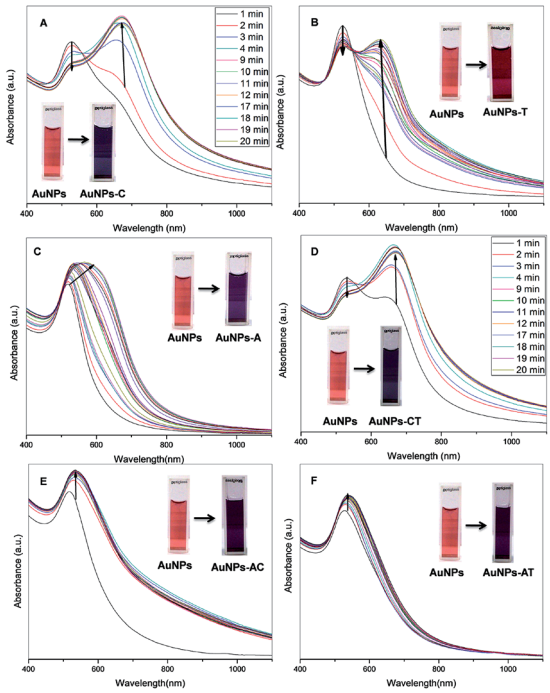

Fig. 1 Kinetics of AuNPs with DNA bases and pair of DNA bases over time. UV-visible kinetics of gold assembly formation upon addition of 30 μL of (A) cytosine (20 mM) (B) thymine (20 mM) (C) adenine (20 mM) into 3 mL AuNPs solution (D) pair of CT (20 mM) (E) pair of AC (20 mM) (F) pair of AT (20 mM) into 3 mL AuNPs solution.

appearance of a broad band at 520 nm after addition of adenine to the gold nanoparticles indicates better interactions. However, precipitation accrued within 8 days after addition of adenine in AuNPs. AuNPs–A has zeta potential of −28 mV, which indicates moderate stability of solution (Fig. S1, ESI†). The degree of interaction of the nucleobases with AuNPs is different which results in different aggregation for different bases. After the addition of DNA bases in AuNPs, pH of the solution remains unchanged (Table S1, ESI†), a deliberate pH change (4–12) may perhaps not bring out any such aggregates. This explains the perception of the study.

The spectral characteristics differ for the paired DNA bases with AuNPs as compared to the mono DNA Bases. The UV-visible spectra for the AuNPs–CT pair wherein, CT is a mixture of cytosine and thymine (20 mM), the CT pair was observed to have a lower adsorption affinity than the individual bases (C and T) and that the adsorption affinity of C was marginally higher than that of T (Fig. 1D). The spectra for the pair of AuNPs–AT had similar spectral features of individual adenine (Fig. 1F). This may be due to the masking effect of adenine. Thymine has lower adsorption affinity than adenine due to the two binding modes in adenine (amine group and ring N atom) while thymine has one binding mode (carbonyl group) (Fig. S4† of FTIR). The spectra of AuNPs–AC showed the intermediate characteristics of C and T, which might be possible due to similar adsorption affinity (Fig. 1E). The zeta-potential values for pair of bases were found in the range of −24.5 to −37.1 mV, confirming a moderate colloidal stability (Fig. S1 and Table S1, ESI†).

The interactions between the gold nanoparticles with DNA bases were analyzed from the FTIR spectra. In AuNPs–C, a remarkable shift was observed in the position and intensity for the C(2)=O(8) group frequency from 1703 (free) to 1645 cm^{-1} (bound to AuNPs). This designated that cytosine binds to AuNPs *via* carbonyl group (Fig. S3 and Table S2, ESI†). The N(3)=C(4) stretching band exhibited a hypsochromic shift from 1536 (free) to 1504 cm^{-1} (bound to AuNPs) which indicates that cytosine binds to AuNPs through N(3) nitrogen atom of the pyrimidine ring (Fig. S2 and Table S2, ESI†). The C(4)–NH_2 stretching band (bound to AuNPs) broadens with respect to the free cytosine which suggests that cytosine can bind to AuNPs through amine group (Fig. S2 and Table S2, ESI†). The lone pair from exocylic nitrogen is also expected to take part in binding with gold nanoparticles.[32] In AuNPs–T, major changes due to increased wavenumbers of both the N–H stretching and bending vibrations, and minor variations of the C=O stretching modes were observed (Fig. S3 and Table S3, ESI†). Also, a remarkable difference was observed in the position and intensity of C(4)=O(8) group (Fig. S4 and Table S3, ESI†). This indicated that thymine binds to AuNPs through the carbonyl group.[33] In AuNPs–A, NH_2 scissoring mode (1779 cm^{-1}) a hypsochromic shift with respect to free adenine (1720 cm^{-1}) (Fig. S4 and Table S4, ESI†) was observed, suggesting that external amino group participated in the binding process with AuNPs.[33] The C–N(7) stretching in five-membered ring shows decrease in intensity and a slight shift from 1595 (free) to 1579 cm^{-1} (bound to AuNPs) (Fig. S4 and Table S4, ESI†), indicating that adenine strongly interacts with the AuNPs through the N(7) nitrogen atom of an imidazole ring (Fig. S6, ESI†).[34–37]

Prominent bands centred at 1761, 1661 and 1345 cm^{-1} were attributed to stretching vibration of C(4)=O(8) of adenine, C–N(7) stretching in five-membered ring[37] of adenine, and C–N stretching of adenine for the AuNPs–AT pair (Fig. S5, ESI†). These bands clearly indicate that adsorption is dominated by A than T in case of AT pair. For the AuNPs–AC pair major bands centred at 1671, 1604 and 1345 cm^{-1} were attributed to stretching vibration of two secondary amide carbonyl C(2)=O(8) groups in cytosine ring, NH_2 scissoring mode, and C–N stretching of adenine (Fig. S6, ESI†). These bands clearly indicate equal adsorption affinity of C and A in case of AC pair. While in case of pair of AuNPs–CT the bands centred at 1770, 1695 and 1345 cm^{-1} were attributed to stretching vibration of two secondary amide carbonyl C(2)=O(8) groups in cytosine ring, and C(4)–NH_2 stretching vibration of cytosine (Fig. S5, ESI†).[32,38] These bands clearly indicate that adsorption is dominated by C than T in case of CT pair.

The TEM study was undertaken to highlight the shape, size and size distribution of the particles. A TEM micrograph of the AuNPs appears as well separated nearly spherical particles (Fig. 2A) with an average size of 6.3 nm. After addition of adenine to the gold nanoparticles solution (Fig. 2B), the particle size was reduced to 4.8 nm indicating an interaction which is supported by UV-Vis spectra. TEM micrograph of AuNPs–T shows aggregation (Fig. 2C) with increase in the particle size (15.5 nm). After addition of cytosine in gold nanoparticles solution (Fig. 2D), the particles seem to be elongated with

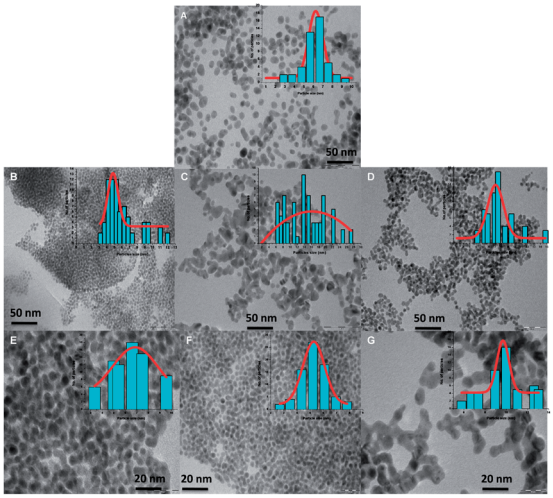

Fig. 2 TEM images and size distributions of gold nanoparticles (A), AuNPs–A (B), AuNPs–T(C), AuNPs–C (D), AuNPs–AT (E), AuNPs–AC (F) and AuNPs–CT (G).

particles size of 7.1 nm. TEM micrographs for the AuNPs–AT, AuNPs–AC and AuNPs–CT pairs show aggregation with the size of 6.7 nm, 6.1 nm and 9.4 nm, respectively (Fig. 2E–G). The addition of mono and paired DNA bases in AuNPs exhibit a significant change in the particle size and a tendency to agglomerate as inferred from the TEM images.

Fig. 3A depicts the electrophoretic patterns for the different AuNPs–DNA bases. A control image of the gel was captured without staining under white light illumination. The image clearly indicates that the functionalized AuNPs (1–7) show almost similar mobility towards anode with the variation in band intensity. Highest band intensity was observed in AuNPs–T and AuNPs–AT systems (Fig. 3B). This study indicates that functionalized AuNPs were negatively charged and show mobility towards anode.

Cellular uptake by cancer cells

The cellular uptake of DNA bases functionalized AuNPs in the human carcinoma cell *viz.* HeLa cells was studied. The bright field images captured exhibit enhanced cellular uptake of functionalized AuNPs uptake compared to AuNPs, as seen in Fig. 4. The cell morphology was observed after the addition of nanoparticles. It is clear from the images that, the cells treated with bare nanoparticles (Fig. 4A) have also reduced in number, indicating that the bare nanoparticles do have some effect on the cell viability. Fig. 4B–G shows the functionalized AuNPs were cytotoxic and enhanced cell death compared to bare AuNPs. Fig. 4E–G shows the presence of pair of DNA bases with AuNPs, particularly AuNPs–AC and AuNPs–CT internalization within the cell (indicated by an arrow).

The key parameter in evaluating biocompatibility was centred on the evaluation of potential cytotoxicity of the nanoparticles. To examine the cytotoxicity in HeLa cell lines, increasing amounts of functionalized AuNPs were incubated and the cell viability was assessed for 24–96 h, expressed as percentage of the untreated control (100% cell viability) by MTT assay. Since the functionalized AuNPs exhibit cellular uptake, the cytotoxic evaluations of these NPs were carried out to quantitate cell death. However, 2 μg mL^{-1} functionalized AuNPs treatment at 24 h, demonstrated 95–97% cell viability in HeLa cell lines (Fig. 5) which further decreases to 52–50% at 48 h and 34–29% at 96 h, respectively. At 24–96 h, the cell viability decreased considerably as the concentration increased up to 30 μg mL^{-1}, almost 48–40% cell viability was observed after 24 h which further decreased to 24–15% for 48 h and 10–5% for 96 h. At 24–96 h, the AuNPs–CT, exhibited highest cell viability

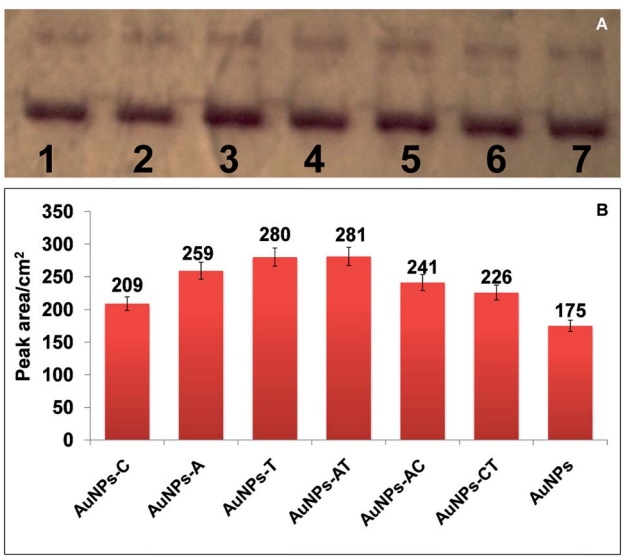

Fig. 3 Gel electrophoresis experiment showing the behaviour of functionalized AuNPs under the effect of an electric field. Panel A shows functionalized AuNPs run through the gel. Panel B shows the plot of band intensity of functionalized AuNPs.

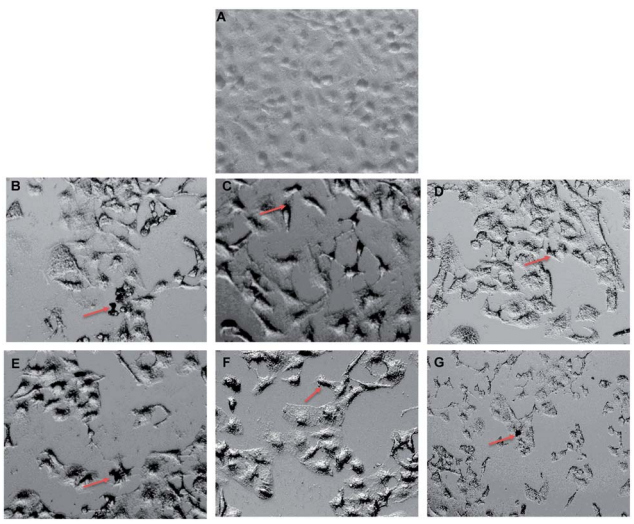

Fig. 4 Bright field microscopic images of functionalized AuNPs into HeLa cell lines after 24 h incubation. The observed black dots (red arrow) indicate the presence of functionalized AuNPs after their internalization into cells.

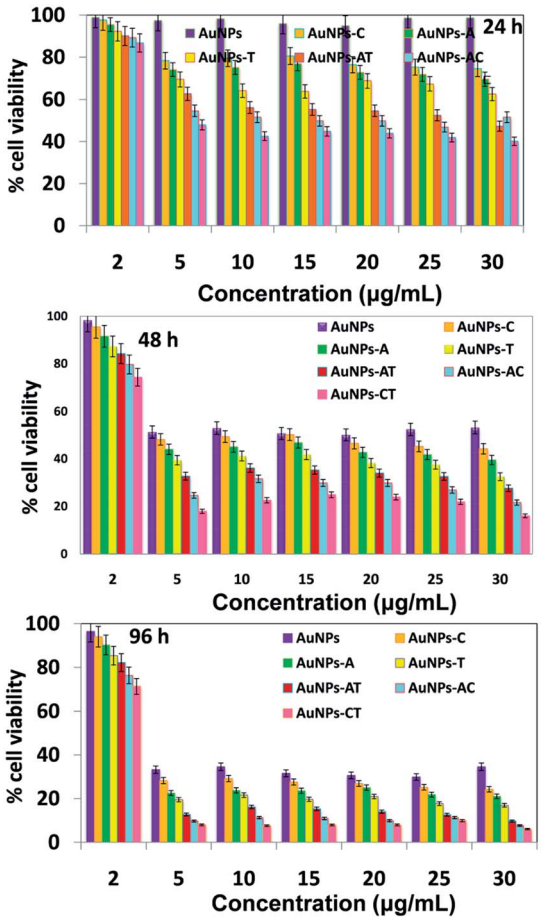

Fig. 5 Cytotoxicity measurements of functionalized AuNPs in HeLa cell lines at various concentrations 2–30 μg mL^{-1} for 24 h, 48 h and 96 h using MTT cell viability assay.

amongst other samples at 30 μg mL^{-1} concentration (Fig. 5). Cell viability of HeLa cells decreased after exposure to functionalized AuNPs, especially at high concentrations.

Cytotoxicity study of functionalized AuNPs was also carried out with healthy cell line (Fig. S7 and S8, ESI†). However, 30 μg mL^{-1} of functionalized AuNPs treatment at 24 h demonstrated 90–70% cell viability in healthy cell lines which further decreases to 89–69% at 48 h (Fig. S7 and S8, ESI†). This result indicates that functionalized AuNPs show high cytotoxicity towards cancer cells (HeLa cells) compared to healthy cells. Also among other NPs, AuNPs–CT show high percentage of cell death in HeLa cell lines (5.97% cell viability at 30 μg mL^{-1} after 96 h). Cytotoxicity study demonstrated that functionalized AuNPs possess the highest toxicity than AuNPs in HeLa cell lines.

Further the AuNPs–DNA bases were tagged with FITC fluorophore to confirm cellular uptake. Fig. 6 shows the cellular uptake of functionalized AuNPs by HeLa cells monitored by fluorescence microscopy. Bright blue fluorescence was observed when cells were incubated with functionalized AuNPs, demonstrating their uptake by the cells. Internalized AuNPs–DNA bases were observed as green colour while the nucleus stained with blue colour. Interestingly, only the nucleus was found to be

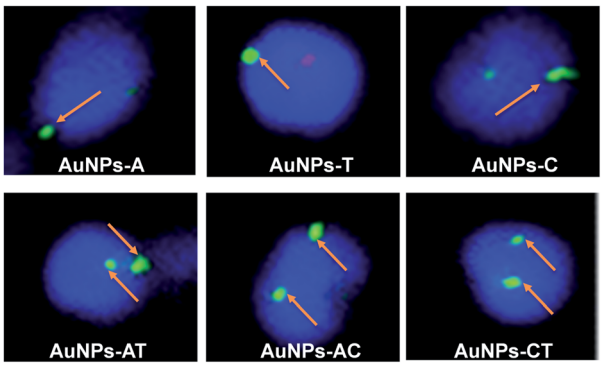

Fig. 6 Fluorescence imaging with DAPI and FITC labelled functionalized AuNPs. The cellular uptake study indicates sufficient functionalized AuNPs were internalized to allow direct visualization (indicated by an arrow).

stained blue, suggesting that these functionalized AuNPs easily enter nucleus of cell. As observed in Fig. 6, the functionalized AuNPs efficiently get internalized within the cells in 4 h, hence making it viable to study the effects of the drug. AuNPs–CT aggregates show complete internalization in the nucleus (Fig. 6).

Quantification of the amount internalized functionalized AuNPs

Microscopic analysis is valuable for obtaining qualitative information on uptake and for intracellular distribution but it only evaluates a comparatively small population of the cells. Hence, a quantitative measurement was essential. Because gold is not found in measurable concentration in mammalian cells, AES can be used to quantify the total amount of gold in a large number of cells and to determine cellular uptake and has sub-ppb detection limits. The amounts of internalized HeLa cells were quantified by MP-AES. The quantification was based on an examination of all exposed cells and thus resulted in higher precision compared to high magnification microscopic image analysis, in which only individual cells were examined. After exposing the cells to functionalized AuNPs for 24 h, the entire cell population was detached and analyzed after lysis to determine the internalized gold concentration. The percentage uptake of AuNPs applied to cells could be calculated, based on the number of AuNPs within the cells and on the total amount applied to the cells.

Fig. 7 depicts the variation in cellular uptake of nanoparticles at 24 h expressed as % particles uptake. The results revealed that nearly 30% to 52% of particles accumulated within the cells for 100 μg mL^{-1} nanoparticles concentration, respectively.

Fig. 7 demonstrates that pair of bases appended AuNPs show higher amount of uptake in HeLa cells. However, the amount of AuNPs within the cells was higher for AuNPs–CT sample (51.43%) among others NPs. MP-AES results indicate that functionalized of AuNPs by a pair of DNA bases can enhance the cellular uptake. Also these functionalized AuNPs were internalized to a greater extent with high cellular uptake than AuNPs

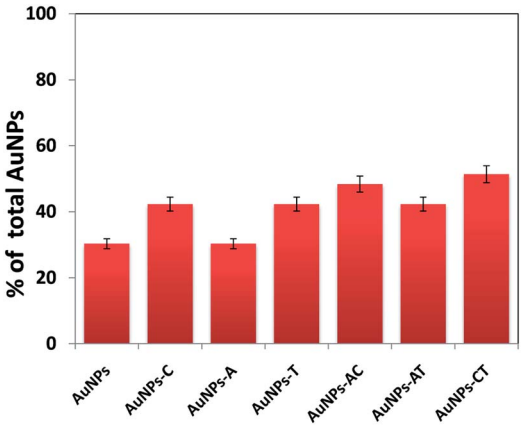

Fig. 7 Quantification of internalized functionalized AuNPs in HeLa cell by MP-AES. Percentage taken up was calculated using gold nanoparticles as a control.

into HeLa cells. However optical microscopy results also support this results that pair of bases functionalized AuNPs demonstrate higher degree of internalization.

Discussion

A typical surface plasmon band of spherical AuNPs is observed due to the collective oscillation of the conduction electrons in the totally symmetric geometry of the particles. Addition of DNA bases into the AuNPs solution generates a new plasmon band along-with the SPR band. The SPR band is assigned to the dipole plasmon excitation of the individual AuNPs, while longitudinal band is assigned to the dipole plasmon resonance appearing due to the aggregation among the individual nanoparticles.[39,40] The appearance of longitudinal band at longer wavelength region and its relative position with different nucleobases could be accounted for within the framework of effective medium theory.[41]

The strength of interaction of the nucleobases with AuNPs may be evaluated on the basis of the appearance of longitudinal band which arises at longer wavelengths. From the optical absorption study it can be inferred that cytosine has strong interactions amongst the DNA bases. The increasing strength of gold–DNA bases can be accounted for the decrease in the interparticle spacing between the particles which is clearly reflected by the position of the extended plasmon band of functionalized AuNPs. The difference in the strength of interaction with AuNPs is likely due to the varying ability of the bases to coordinate the AuNPs surface, this leads to possible nonspecific chemical interactions outcome in different aggregation mechanisms for different nucleobases.

In cytosine, the available lone pair from exocyclic nitrogen takes part in binding gold. It can generate a lesser amount of canonical structures than adenine. Thus, AuNPs would strongly interact with cytosine. The best aggregation takes place in the case of cytosine as nitrogen and oxygen become preferred donors. As cytosine contains electron rich N and O atoms, the charge-transfer interactions from the lone pair on O are expected to take part.[42] Whereas thymine has no such exocyclic nitrogen and presumably the ring nitrogen does not take part in bonding so the entire bonding takes place through O atoms. IR studies further confirm that the binding is preferred through the carbonyl (C(4)═O(8)) group with gold particles. Hence the orientation of the molecular plane becomes perpendicular to the surface of gold nanoparticles instead of being parallel as in case of cytosine and adenine.[33] In adenine, the presence of the aromatic benzene ring together with the heterocyclic five-membered ring provides additional stability due to delocalization of the electron density.[43] Purine bases are less aromatic compared to pyrimidine bases as reported earlier by the Sharma group. Thus both become more aromatic on complexation with gold atoms. Generally the gold atom bound to an electron rich site is found to withdraw electrons and acquire a negative charge. The carbon atoms of the adenine loose a lesser amount of electron density, whereas the nitrogen atoms loose a greater charge, this is due to the vicinity of the gold atoms to the N atoms. A significant charge transfer takes place from the lone pair of N in adenine to gold. In adenine the exocyclic nitrogen is adjacent to two almost equivalent ring nitrogens in its six-membered skeleton which might be the reason for better interaction with gold surface.[42]

This study suggests predominant interaction of the gold atoms with electron rich regions in the bases involving mainly the hetero atoms like N and O. Thymine exhibits weakest interaction with the metal nanoparticles which is in agreement with the previous results (C > G > A > T).[33,40,44,45] It is well established in the literature that amines can bind exceptionally strongly with metal nanoparticles.[46] Recent DFT and Post Hartree–Fock calculations have shown that the interaction of the DNA bases with the gold surface is dominated by dispersion interactions.[47]

It is well established that the particle charge and colloidal stability is of great importance in the cellular uptake studies.[48] The zeta-potential values were found in the range of −53 to −24.5 mV. The negative zeta potential values for all functionalized AuNPs indicate the relative stability of these particles in the dispersion medium. The zeta-potential values of the AuNPs followed the order AuNPs–T < AuNPs–AT < AuNPs–AC < AuNPs–C < AuNPs–A < AuNPs–CT, the rise in the zeta-potential value can be associated with the formation of small nanoparticle arrangements, causing a light scattering increase and a mobility bias by the largest particles in the poly-dispersed sample.[49,50]

As reported earlier, AuNPs have little toxic effects due to the nature of inert elements. AuNPs when functionalized with the suitable surface moieties, can readily penetrate living cells.[17] The cytotoxicity of the AuNPs has been previously reported to be dependent on AuNPs concentration, time of treatment, and cell type.[51–54] For clinical applications, it is very essential that the nanoparticles show efficient cellular uptake and easy clearance.

The bright field microscopic images indicate AuNPs–DNA bases uptake in the HeLa cell lines (Fig. 4). The observed black dots (Fig. 4) indicate the presence of functionalized AuNPs after their internalization into the cells. This study was further confirmed by tagging the AuNPs–DNA bases with FITC. The

cellular uptake study indicates sufficient functionalized AuNPs internalized within the cell to allow direct visualization (green dots) using fluorescence microscopy, as shown in Fig. 6. The mono and paired DNA bases functionalized AuNPs were able to enter the cells after 4 h of treatment. Thus, the cellular uptake and cell viability studies suggest that functionalized AuNPs are suitable for *in vivo* applications. The uptake of gold nanoparticles is mediated by the adsorption of serum proteins onto the gold surface *via* the mechanism of receptor-mediated endocytosis.[55–57] However, our results are consistent with earlier data showing that in human dermal fibroblasts,[58] leukemia cells,[59] human hepatocellular cells,[60] rat alveolar macrophages and epithelial type-I cells,[61] in mouse dendritic cells and fibroblasts,[62,63] gold nanoparticles were internalized. The uptake of AuNPs seems to depend on the surface structure of NPs. The authors concluded that negatively charged gold nanoparticles interacted with proteins on the cell surface that might promote an uptake process.

MP-AES study suggested that functionalized AuNPs were internalized to a greater extent with high cellular uptake than AuNPs. High percentage of uptake of functionalized AuNPs would be of great importance for medical applications. Fazal and co-worker also demonstrated that AuNPs synthesized by green route show cellular uptake 47% to 67% in A431 cell lines.[64]

In addition to the charge effect, a size effect also plays a vital role in cellular internalization of gold nanoparticles. Nel group extensively discussed the biophysico-chemical interactions at the nano-bio interface. In addition to the various forces involved in the adsorption to the cell membrane, the diameter of the nanoparticle was of major importance in promoting internalization into the cell.[65] Previous studies have found that, AuNPs of less than 20 nm are more suitable for biological application compared to particles of bigger sizes, as their cellular uptake is higher and they can cross the blood–brain barrier in animal model.[66,67] The present TEM study also indicates that the functionalized AuNPs are below 20 nm.

Conclusions

We have been able to successfully design AuNPs appended with DNA bases that tend to aggregate. This property of aggregation renders suitable property to the appended AuNPs which helps in cell internalization and enhanced cytotoxicity. In HeLa cell lines the paired DNA bases functionalized AuNPs were internalized to a higher degree even after a short exposure time of 4 h, as would be expected due to interactions with the anionic cell membrane. The damage rendered to the cell can be corroborated to the accumulation of the AuNPs–DNA bases within the cell. Our studies have indicated that these functionalized AuNPs are able to penetrate into the nucleus of HeLa cell. This work can further be extended to various applications in the field of nanomedicine and nanobiotechnology.

Acknowledgements

Financial support by UGC-UPE (Bio-Nano), Savitribai Phule Pune University is duly acknowledged. A. A. Khan/Authors acknowledge the Institute of Bioinformatics and Biotechnology, Savitribai Phule Pune University for providing the animal tissue culture facility. Authors are also thankful to venture centre, NCL, Pune for MP-AES analysis and Ms Edna Joseph for analysis as well as helpful discussion related to MP-AES.

References

1 H. Gao, Z. Yang, S. Zhang, S. Cao, S. Shen, Z. Pang and X. Jiang, *Sci. Rep.*, 2013, **3**, 2534–2542.
2 J. Shi, Z. Xiao, N. Kamaly and O. C. Farokhzad, *Acc. Chem. Res.*, 2011, **44**, 1123–1134.
3 A. Arnid, A. Malugin and H. HamidrezaGhandehari, *J. Appl. Toxicol.*, 2010, **30**, 212–217.
4 M. C. Daniel and D. Astruc, *Chem. Rev.*, 2004, **104**, 293–346.
5 P. K. Jain, I. H. El-Sayed and M. A. El-Sayed, *Nano Today*, 2007, **2**, 18–29.
6 X. Huang, P. K. Jain, I. H. El-Sayed, M. A. Mostafa and M. A. El-Sayed, *Nanomedicine*, 2007, **2**, 681–693.
7 K. Sokolov, M. Follen, J. Aaron, I. Pavlova, A. Malpica, R. Lotan and R. Richards-Kortum, *Cancer Res.*, 2003, **63**, 1999–2004.
8 I. H. El-Sayed, X. Huang and M. A. El-Sayed, *Cancer Lett.*, 2005, **239**, 129–135.
9 T. B. Huff, L. Tong, Y. Zhao, M. N. Hansen, J. X. Cheng and A. Wei, *Nanomedicine*, 2007, **2**, 125–132.
10 D. Neal, L. Hirsch, N. Halas, J. Payne and J. West, *Cancer Lett.*, 2004, **209**, 171–176.
11 I. H. El-Sayed, X. Huang and M. A. El-Sayed, *Cancer Lett.*, 2006, **209**, 171–176.
12 W. Huang, W. Qian, P. K. Jain and M. A. El-Sayed, *Nano Lett.*, 2007, **7**, 3227–3234.
13 G. Saikia, A. Murugadoss, P. J. Sarmah, A. Chattopadhyay and P. K. Iyer, *J. Phys. Chem. B*, 2010, **114**, 14821–14826.
14 E. E. Connor, J. Mwamuka, A. Gole, C. J. Murphy and M. D. Wyatt, *Small*, 2005, **1**, 325–327.
15 D. P. O'Neal, L. R. Hirsch, N. J. Halas, J. D. Payne and J. L. West, *Cancer Lett.*, 2004, **209**, 171–176.
16 G. F. Paciotti, L. Myer, D. Weinreich, D. Goia, N. Pavel, R. E. McLaughlin and L. Tamarkin, *Drug Delivery*, 2004, **11**, 169–183.
17 Z. Krpetic, S. Saleemi, I. A. Prior, V. See, R. Qureshi and M. Brust, *ACS Nano*, 2011, **5**, 5195–5201.
18 J. Chen, A. Zheng, A. Chen, Y. Gao, C. He, X. Kai, G. Wu and Y. Chen, *Anal. Chim. Acta*, 2007, **599**, 134–142.
19 H. Chang, T. Hsiung, Y. Huang and C. Huang, *Environ. Sci. Technol.*, 2011, **45**, 1534–1539.
20 J. P. Lafleur, S. Senkbeil, T. G. Jensen and J. P. Kutter, *Lab Chip*, 2012, **12**, 4651–4656.
21 S. Hegde, S. Kapoor, S. Joshi and T. Mukherjee, *J. Colloid Interface Sci.*, 2006, **297**, 637–643.
22 H. Colfen and S. Mann, *Angew. Chem.*, 2003, **42**, 2350–2365.
23 K. R. Dutta, P. K. Sharma and A. C. Pandey, *Appl. Phys. Lett.*, 2010, **97**, 253702–253705.
24 P. S. Ghosh, C. K. Kim, G. Han, N. S. Forbes and V. M. Rotello, *ACS Nano*, 2008, **2**, 2213–2218.

25 M. S. Han, A. K. R. Lytton-Jean and C. A. Mirkin, *J. Am. Chem. Soc.*, 2006, **128**, 4954–4955.
26 M. S. Han, A. K. R. Lytton-Jean, B. K. Oh, J. Heo and C. A. Mirkin, *Angew. Chem., Int. Ed.*, 2006, **118**, 1839–1842.
27 A. K. R. Lytton-Jean, M. S. Han and C. A. Mirkin, *Anal. Chem.*, 2007, **79**, 6037–6041.
28 H. Pan, R. Cui and J. Zhu, *J. Phys. Chem. B*, 2008, **112**, 16895–17001.
29 J. A. Creighton, C. G. Blatchford and M. G. Albrecht, *J. Chem. Soc., Faraday Trans. 2*, 1979, **75**, 790–798.
30 S. Basu, S. Jana, S. Pande and T. Pal, *J. Colloid Interface Sci.*, 2008, **321**, 288–293.
31 (*a*) S. P. Robinson and A. J. Stagg, *Dendritic cell protocols*, Humana Press, New Jersey, 2001, p. 470; (*b*) E. Ulukaya, M. Colakogullari and E. J. Wood, *Chemotherapy*, 2004, **50**, 43–50.
32 J. Kundu, O. Neumann, B. G. Janesko, D. Zhang, S. Lal, A. Barhoumi, G. F. Scuseria and N. J. Halas, *J. Phys. Chem. C*, 2009, **113**, 14390–14397.
33 N. H. Jang, *Bull. Korean Chem. Soc.*, 2002, **23**, 1790–1800.
34 A. McNutt, S. Haq and R. Raval, *Surf. Sci.*, 2003, **531**, 131–144.
35 M. Ostblom, B. Liedberg, L. M. Demers and C. A. Mirkin, *J. Phys. Chem. B*, 2005, **109**, 15150–15160.
36 T. Yamada, K. Shirasaka, A. Takano and M. Kawai, *Surf. Sci.*, 2004, **561**, 233–247.
37 Q. Chen, D. J. Frankel and N. V. Richardson, *Langmuir*, 2002, **18**, 3219–3225.
38 J. S. Arikrishnan, S. K. T. Sheerin, M. Murugavelu and B. Karthikeyan, *Indian J. Chem., Sect. A: Inorg., Bio-inorg., Phys., Theor. Anal. Chem.*, 2010, **50**, 46–50.
39 T. Jensen, L. Kelly, A. Lazarides and G. C. Schatz, *J. Cluster Sci.*, 1999, **10**, 295–317.
40 S. K. Ghosh and T. Pal, *Chem. Rev.*, 2007, **107**, 4797–4862.
41 J. C. Maxwell-Garnett, *Philos. Trans. R. Soc., B*, 1904, **203**, 385–420.
42 H. Singh, S. Sharma and H. Singh, *J. Chem. Theory Comput.*, 2007, **3**, 2301–2311.
43 I. V. Omelchenko, O. V. Shishkin, L. Leonid Gorb, J. Leszczynski, S. Fiase and P. Bultinck, *Phys. Chem. Chem. Phys.*, 2011, **13**, 20536–20548.
44 S. Gourishankar, S. Shukla, K. N. Ganesh and M. Sastry, *J. Am. Chem. Soc.*, 2004, **126**, 13186–13187.
45 L. M. Demers, M. Ostblom, H. Zhang, N. H. Jang, B. Liedberg and C. A. Mirkin, *J. Am. Chem. Soc.*, 2002, **124**, 11248–11249.
46 S. Nath, S. K. Ghosh, S. Kundu, S. Praharaj, S. Panigrahi and T. Pal, *J. Nanopart. Res.*, 2006, **8**, 111–116.
47 S. Piana and A. Bilic, *J. Phys. Chem. B*, 2006, **110**, 23467–23471.
48 Y. Zhang, M. Yang, J. H. Park, J. Singelyn, H. Ma, M. J. Sailor, E. Ruoslahti, M. Ozkan and C. Ozkan, *Small*, 2009, **5**, 1990–1996.
49 T. L. Doane, C. H. Chuang, R. J. Hill and J. C. Burda, *Acc. Chem. Res.*, 2012, **45**, 317–326.
50 S. Avvakumova, G. Scarib and F. Porta, *RSC Adv.*, 2012, **2**, 3658–3661.
51 C. Boyoglu, Q. He, G. Willing, S. Boyoglu-Barnum, V. A. Dennis, S. Pillai and S. R. Singh, *ISRN Nanotechnol.*, 2013, **2013**, 1–13.
52 K. Katti, N. Chanda and R. Shukla, *Int. J. Green Nanotechnol.*, 2009, **1**, 39–52.
53 R. Shukla, S. K. Nune and N. Chanda, *Small*, 2008, **4**, 1425–1436.
54 S. P. Chandran, M. Chaudhary, R. Pasricha, A. Ahmad and M. Sastry, *Biotechnol. Prog.*, 2006, **22**, 577–583.
55 B. D. Chithrani, A. A. Ghazani and W. C. W. Chan, *Nano Lett.*, 2006, **6**, 662–668.
56 B. D. Chithrani and W. C. W. Chan, *Nano Lett.*, 2007, **6**, 1542–1550.
57 A. M. Alkilany, P. K. Nagaria, C. R. Hexel, T. J. Shaw, C. J. Murphy and M. D. Wyatt, *Small*, 2009, **5**, 701–708.
58 N. Pernodet, X. Fang, Y. Sun, A. Bakhtina, A. Ramakrishnan, J. Sokolov, A. Ulman and M. Rafailovich, *Small*, 2006, **2**, 766–773.
59 E. E. Connor, J. Mwamuka, A. Gole and C. J. Murphy, *Small*, 2005, **1**, 325–327.
60 C. J. Gannon, C. R. Patra, R. Bhattacharya, P. Mukherjee and S. A. Curley, *J. Nanobiotechnol.*, 2008, **6**, 1–9.
61 S. Takenaka, E. Karg, W. G. Kreyling, B. Lentner, W. Moller, M. Behnke-Semmler, L. Jennen, A. Walch, B. Michalke and P. Schramel, *Inhalation Toxicol.*, 2006, **18**, 733–740.
62 A. Verma, O. Uzun, Y. Hu, H. S. Han, N. Watson, S. Chen, D. J. Irvine and F. Stellacci, *Nat. Mater.*, 2008, **7**, 588–595.
63 C. Freese, M. I. Gibson, H. A. Klok, R. E. Unger and C. J. Kirkpatrick, *Biomacromolecules*, 2012, **13**, 1533–1543.
64 S. Fazal, A. Jayasree, S. Sasidharan, M. Koyakutty, S. V. Nair and D. Menon, *ACS Appl. Mater. Interfaces*, 2014, **6**, 8080–8089.
65 A. E. Nel, L. Madler, D. Velegol, T. Xia and E. M. V. Hoek, *Nat. Mater.*, 2009, **8**, 543–557.
66 M. Semmler-Behnke, W. G. Kreyling and J. Lipka, *Small*, 2008, **4**, 2108–2111.
67 H. Jin, D. A. Heller, R. Sharma and M. S. Strano, *ACS Nano*, 2009, **3**, 149–158.

